

Why the Casimir Force for Magnetic Metals Computed by the Lifshitz Theory Using the Drude Model Disagrees with the Measurement Data

G. L. Klimchitskaya,^{1,2} C. C. Korikov,³ and V. M. Mostepanenko^{1,2}

¹*Central Astronomical Observatory at Pulkovo of the Russian Academy of Sciences, St.Petersburg, 196140, Russia*

²*Peter the Great Saint Petersburg Polytechnic University, Saint Petersburg, 195251, Russia*

³*Moscow Center for Advanced Studies, Kulakova Str. 20, 123592 Moscow, Russia*

We consider the Casimir force in configurations with magnetic metal plates and analyze the reasons why the predictions of the Lifshitz theory using the dielectric permittivity of the Drude model are inconsistent with the measurement data. For this purpose, the contributions of the electromagnetic waves with the transverse magnetic and transverse electric polarizations to the Casimir force are computed using the Lifshitz theory expressed in terms of the pure imaginary Matsubara frequencies. Furthermore, the fractions of the evanescent and propagating waves in these contributions are found using an equivalent formulation of the Lifshitz theory along the real frequency axis. All computations are performed for Au-Ni and Ni-Ni plates using the Drude model and the experimentally consistent plasma model over the separation region from 0.5 to 6 μm , where the total force value is determined by conduction electrons. It is shown that the transverse magnetic contribution to the Casimir force does not depend on the used model of the dielectric permittivity, so that the total difference between the predictions of the Lifshitz theory using the Drude model and the measurement data is determined by the transverse electric contribution. In doing so, as opposed to the case of nonmagnetic metals, both fractions of the evanescent and propagating waves in this contribution depend on the model of the dielectric permittivity used in computations, whereas the magnetic properties of the plate metal influence the Casimir force solely through the fraction of propagating waves in the transverse electric contribution. The issue of a more adequate theoretical description of the electromagnetic response of magnetic metals is discussed.

I. INTRODUCTION

The first quantum theory by Werner Heisenberg [1] and Erwin Schrödinger [2], quantum mechanics, created one hundred years ago laid the groundwork for an understanding of many physical phenomena which could not be described on the basis of standard approaches developed in the framework of Newtonian mechanics and Maxwell's electrodynamics. One of these phenomena is the van der Waals force playing the crucial role in diverse fields of physics, chemistry, biology, and nanotechnology [3]. The nonrelativistic theory of the van der Waals forces was created by London [4] in 1930 on the basis of quantum mechanics. A generalization of the van der Waals force for larger separations between the interacting bodies was suggested by Casimir [5] for the case of two ideal metal planes. The Casimir force arises due to a change in the spectrum of zero-point oscillations of quantized fields caused by the boundary conditions. The unified theory of the van der Waals and Casimir forces was created by Lifshitz [6–8] within the formalism which is essentially the thermal quantum field theory.

With the advent of high-precision laboratory techniques using the micromechanical torsional oscillators, the Casimir force acting between the Au-coated surfaces of a plate and a microsphere was measured by R.S. Decca with increased precision, and the obtained measurement data were compared with theoretical predictions of the Lifshitz theory [9–12]. The Lifshitz theory represents the Casimir force as a sum of integrals where the integrands are expressed via the dielectric permittivities $\varepsilon_l^{(m)} = \varepsilon^{(m)}(i\xi_l)$ of two interacting bodies, $m = 1, 2$, calculated at the pure imaginary Matsubara frequencies $i\xi_l = 2\pi ik_B T l / \hbar$ where k_B is the Boltzmann constant, T is the temperature and $l = 1, 2, 3, \dots$ [6–8, 13]. The values of $\varepsilon_l^{(m)}$ for two Au bodies $\varepsilon_l^{(1)} = \varepsilon_l^{(2)} = \varepsilon_l^{\text{Au}}$ are calculated by using the Kramers-Kronig relation expressing $\varepsilon_l^{(m)}$ via $\text{Im } \varepsilon^m(\omega)$, and the values of $\varepsilon^{(m)}$ at real frequencies ω are obtained from the measured complex indices of refraction $n^{(m)}(\omega)$ of the interacting bodies (see the tables in Ref. [14]).

The values of $n^{(m)}(\omega)$ and, thus, $\varepsilon^{(m)}(\omega)$ can be, however, measured only over a restricted frequency region from ω_{\min} to ω_{\max} . For instance, for Au $\hbar\omega_{\min} = 0.125 \text{ eV}$ and $\hbar\omega_{\max} = 10^4 \text{ eV}$ [14]. In so doing, ω_{\max} is usually sufficiently large, so that one does not need to know the values of $\varepsilon^{(m)}(\omega)$ for $\omega > \omega_{\max}$ in order to calculate the Casimir force with the required accuracy. This is not the case for the region of low frequencies $\omega < \omega_{\min}$, where one must know $\varepsilon^{(m)}(\omega)$ for calculating the Casimir force by the Lifshitz theory. This problem is usually solved by making an extrapolation of $\text{Im } \varepsilon^{(m)}(\omega)$ obtained from the optical data for the complex index of refraction to lower frequencies by means of the dielectric permittivity of the Drude model, which provides much tested description of the conduction electrons in nonmagnetic metals.

Surprisingly, it was found that the predictions of the Lifshitz theory calculated in this way are excluded by the measurement data for the Casimir force at the confidence level up to 99.9% [9–12]. Of even greater surprise is the fact that if the optical data related to the core electrons alone are extrapolated to lower frequencies by means of the dielectric permittivity of the dissipationless plasma model, the predictions of the Lifshitz theory agree closely with the measurement data. This agreement is reached by disregarding the optical data in the frequency region $(\omega_{\min}, \omega_1)$, where ω_1 corresponds to the first absorption band of Au determined by core electrons, and extrapolating the obtained $\text{Im } \varepsilon^{(m)}(\omega)$ to the interval $\omega < \omega_1$ by zero because the dielectric

permittivity of the plasma model is real. In this case, $\varepsilon^{(m)}(i\xi_l)$ is found from the Kramers-Kronig relation for functions having the double pole at zero frequency as it holds for the plasma model (see Refs. [13, 15] for details).

An extrapolation of the optical data caused by the core electrons to lower frequencies by means of the plasma model was often considered as unjustified [16–20] because this model disregards the relaxation properties of conduction electrons and is physically applicable only at very high frequencies (for instance, in the region of infrared optics), where the relaxation properties of conduction electrons do not play any role. In subsequent experiments performed by U. Mohideen with Au surfaces using an atomic force microscope [21–24] and by R.S. Decca using a micromechanical torsional oscillator [25] the role of all possible background effects was carefully analyzed and excluded. It was confirmed with certainty that the Lifshitz theory is consistent with the measurement data if it uses an extrapolation of the optical data by means of the plasma model and is inconsistent with the same data if the Drude model is used. Furthermore, it was shown that an entropy of the Casimir interaction computed using the Lifshitz theory violates the third law of thermodynamics (the Nernst heat theorem) for metals with perfect crystal lattices if the Drude model is used and is thermodynamically consistent when one uses the plasma model (see Refs. [13, 15] for a review). This situation was often called "the Casimir puzzle" [26–28].

Many attempts to solve the Casimir puzzle have been undertaken on both the theoretical and experimental sides. Specifically, the more exact models of surface roughness were suggested [29–33], much attention was paid to a rigorous generalization of the Lifshitz theory for the configuration of a sphere above a plate used in experiments [34–50], the corrections due to surface patches [51–53] and variations of the optical data [54–57] in the measured and calculated Casimir forces were investigated, as well as the role of spatial dispersion in the region of the anomalous skin effect [58–60] (see the review [61] for details). However, the contradiction between experiment and theory was left in place.

On this point, an important progress was reached in investigating the frequency region which determines a difference in the theoretical predictions of the Lifshitz theory using extrapolations of the optical data of metallic plates by means of the Drude and plasma models. Although in almost all computations the Lifshitz formula written in terms of the pure imaginary Matsubara frequencies has been used, there is a mathematically equivalent formulation along the real frequency axis.

In Refs. [62, 63] it was shown that a difference between the theoretical predictions for the Casimir force using the Drude and plasma extrapolations of the optical data of nonmagnetic metals originates from the modes with the transverse electric polarization at low ω . This difference was also attributed to the contribution of Foucault currents [64, 65]. Moreover, at separations larger than the thermal length, which is equal to $6 \mu\text{m}$ at $T = 300 \text{ K}$, it was demonstrated [66–68] that this difference is fully determined by the contribution of evanescent waves with the transverse electric polarization (recall that for the propagating waves $k_\perp \leq \omega/c$, where k_\perp is the magnitude of the wave vector projection on the Casimir plates, but for the evanescent ones the inequality $k_\perp > \omega/c$ holds).

Finally, in Ref. [69], by using the Lifshitz formula along the real frequency axis, it was shown that for Au plates within the wide separation region from 0.5 to $4 \mu\text{m}$, where the Casimir force is fully determined by conduction electrons, the difference in theoretical predictions using the Drude and plasma models results from the transverse electric evanescent waves. This result was correlated with the fact that for nonmagnetic metals the Drude model is much-tested only in the region of propagating waves with any polarization. For the transverse magnetic evanescent waves, there are also a few tests in the physics of surface plasmons polaritons [70] and in the near-field optical microscopy [71, 72]. The phenomena of total internal reflection and frustrated total internal reflection [73–75] give the possibility to verify the Drude model for both polarizations of the evanescent electromagnetic waves, but for k_\perp only slightly exceeding ω/c . For this reason, Ref. [69] concluded that the experiments [9–12, 21–25] on measuring the Casimir force between Au surfaces invalidate the Drude model in the region of transverse electric evanescent waves. As to the propagating waves of both polarizations and the transverse magnetic evanescent waves, in these regions of frequencies the Drude model can be safely used when calculating the Casimir force between nonmagnetic metals with no contradiction with the measurement data.

In Refs. [67, 68], the novel experiment in the field of classical electrodynamics was proposed which allows to independently check the Drude model by measuring the lateral component of magnetic field emitted by the oscillating magnetic dipole and reflected from a nonmagnetic metallic surface. It was shown that this component is fully determined by the transverse electric evanescent waves. This experiment has been already performed by U. Mohideen [76] and demonstrated a failure of the Drude model for transverse electric evanescent waves.

Measurements of the Casimir force with magnetic materials are of particular value because in this case the theoretical predictions using the Drude and plasma extrapolations of the optical data interchange their places. Thus, the gradient of the Casimir force, which is the most precisely measured quantity in the sphere-plate geometry, computed using the Drude model for two Au bodies is smaller than that computed using the plasma model. On the contrary, for two bodies made of magnetic metal Ni the gradient of the Casimir force computed using the Drude model is larger than that found by means of the plasma model.

In the experiments performed by means of an atomic force microscope, the gradient of the Casimir force was measured between Au-Ni and Ni-Ni surfaces [77–79]. It was shown that the theoretical predictions using extrapolations of the optical data for Au and Ni to low frequencies by the Drude model are excluded by the measurement data, whereas the predictions using the plasma model are experimentally consistent. In the seminal differential measurement of the Casimir force between either Au- or Ni-coated sphere and the rotating disk with periodic sectors made of Au or Ni performed by R.S. Decca using a micromechanical torsional oscillator [80], the theoretical predictions using the Drude and plasma model extrapolations differ by up to a factor of

1000. As a result, the extrapolation using the Drude model was unequivocally ruled out and the extrapolation by the plasma model was found to be in good agreement with the measurement data.

In this article, we investigate what regions of real frequencies are responsible for a disagreement between the theoretical predictions for the Casimir force obtained using the Drude model in configurations with magnetic metals and the measurement data. For this purpose, we compute the transverse magnetic and transverse electric contributions to the Casimir force for both the evanescent and propagating waves in configurations of Au-Ni and Ni-Ni plates using the Lifshitz formula along the real frequency axis. All computations are repeated using the Drude and plasma models within the separation region from 0.5 to 6 μm where the core electrons do not contribute to the force value.

According to our results, the transverse magnetic contribution to the Casimir force does not depend on whether the Drude or the plasma model is used in computations and on the values of magnetic permeabilities of the plate materials. However, the transverse electric contribution is highly dependent on the model of the dielectric permittivity used. In doing so, the parts of the transverse electric contributions determined by the propagating waves computed using the Drude or the plasma models fully determine a dependence of the Casimir force on magnetic properties. Thus, the difference between the theoretical Casimir forces with magnetic metals when using the Drude and plasma models originate from the contribution of transverse electric waves. Keeping in mind that the experimentally consistent theory for both nonmagnetic and magnetic metals uses the plasma model, one concludes that for magnetic materials the Drude model in the region of transverse electric waves is not accurate enough. The question on how the Drude model should be modified in this region for the case of magnetic materials is discussed.

The article is organized as follows. In Section 2, the transverse magnetic and transverse electric contributions to the Casimir force between Au-Ni and Ni-Ni plates are computed. Section 3 briefly presents the Lifshitz formula written in terms of real frequencies and the concepts of the propagating and evanescent waves. In Section 4, the fractions due to evanescent and propagating waves in the transverse magnetic contribution to the Casimir force are found for Au-Ni and Ni-Ni plates. In Section 5, the same is done for the transverse electric contribution. Section 6 contains a discussion, and we finish with the conclusions in Section 7.

II. CONTRIBUTIONS OF TRANSVERSE MAGNETIC AND TRANSVERSE ELECTRIC POLARIZATIONS TO THE CASIMIR FORCE FOR AU-NI AND NI-NI PLATES IN THE FORMALISM OF IMAGINARY FREQUENCIES

We consider the Casimir force acting between two parallel metallic plates spaced a apart at temperature T in thermal equilibrium with the environment. In the first case, one plate is made of nonmagnetic metal Au and another one of magnetic (but not magnetized) metal Ni. In the second case, both plates are made of Ni. These plates are assumed to be sufficiently thick in order that they could be considered as the semispaces. When calculating the Casimir force between good metals, this condition is satisfied for the plates of more than 100 nm thickness [13].

According to the Lifshitz formula written in terms of the pure imaginary Matsubara frequencies, the Casimir force per unit area of the plates can be presented as the sum of two contributions due to the electromagnetic waves with transverse magnetic (TM) and transverse electric (TE) polarizations

$$F(a, T) = F_{\text{TM}}(a, T) + F_{\text{TE}}(a, T). \quad (1)$$

In the modern notations using the concept of reflection coefficients, these contributions take the form [13]

$$F_{\text{TM,TE}}(a, T) = -\frac{k_B T}{\pi} \sum_{l=0}^{\infty} \left(1 - \frac{\delta_{l0}}{2}\right) \int k_{\perp} dk_{\perp} q_l \frac{r_{\text{TM,TE}}^{(1)}(i\xi_l, k_{\perp}) r_{\text{TM,TE}}^{(2)}(i\xi_l, k_{\perp}) e^{-2aq_l}}{1 - r_{\text{TM,TE}}^{(1)}(i\xi_l, k_{\perp}) r_{\text{TM,TE}}^{(2)}(i\xi_l, k_{\perp}) e^{-2aq_l}}. \quad (2)$$

Here, k_B is the Boltzmann constant, δ_{lk} is the Kronecker symbol,

$$\xi_l = \frac{2\pi k_B T l}{\hbar}, \quad l = 0, 1, 2, \dots, \quad q_l = \left(k_{\perp}^2 + \frac{\xi_l^2}{c^2}\right)^{1/2}, \quad (3)$$

and the reflection coefficients for the TM and TE polarizations are given by

$$r_{\text{TM}}^{(m)}(i\xi_l, k_{\perp}) = \frac{\varepsilon^{(m)}(i\xi_l) q_l - p_l^{(m)}}{\varepsilon^{(m)}(i\xi_l) q_l + p_l^{(m)}}, \quad r_{\text{TE}}^{(m)}(i\xi_l, k_{\perp}) = \frac{\mu^{(m)}(i\xi_l) q_l - p_l^{(m)}}{\mu^{(m)}(i\xi_l) q_l + p_l^{(m)}}, \quad (4)$$

where

$$p_l^{(m)} = \left[k_{\perp}^2 + \varepsilon^{(m)}(i\xi_l) \mu^{(m)}(i\xi_l) \frac{\xi_l^2}{c^2}\right]^{1/2}, \quad (5)$$

$\varepsilon^{(m)}(\omega)$ and $\mu^{(m)}(\omega)$ are the dielectric permittivity and magnetic permeability of the first ($m = 1$) and second ($m = 2$) plates. In the first case considered below, $\varepsilon^{(1)}(\omega) = \varepsilon^{\text{Au}}(\omega)$, $\mu^{(1)}(\omega) = 1$, $\varepsilon^{(2)}(\omega) = \varepsilon^{\text{Ni}}(\omega)$ and $\mu^{(2)}(\omega) = \mu^{\text{Ni}}(\omega)$. In the second case $\varepsilon^{(1)}(\omega) = \varepsilon^{(2)}(\omega) = \varepsilon^{\text{Ni}}(\omega)$ and $\mu^{(1)}(\omega) = \mu^{(2)}(\omega) = \mu^{\text{Ni}}(\omega)$.

We performed computations of the Casimir force per unit area (1) and the transverse magnetic and transverse electric contributions to it (2) for the Au-Ni and Ni-Ni plates at $T = 300$ K within the separation region from 0.5 to 6 μm . In this region of relatively large separations, the bound (core) electrons do not contribute to the Casimir force and one can use in computations the dielectric permittivities caused by only the conduction electrons [13]. Below we use the permittivities of either the Drude or the plasma model at the pure imaginary Matsubara frequencies

$$\varepsilon_D^{(m)}(i\xi_l) = 1 + \frac{\omega_p^{(m)2}}{\xi_l[\xi_l + \gamma^{(m)}(T)]}, \quad \varepsilon_p^{(m)}(i\xi_l) = 1 + \frac{\omega_p^{(m)2}}{\xi_l^2}. \quad (6)$$

For the Au-Ni plates we have the value of the plasma frequency $\hbar\omega_p^{(1)} = 9.0$ eV and the relaxation parameter $\hbar\gamma^{(1)}(T = 300 \text{ K}) = 0.035$ eV for Au [81] and $\hbar\omega_p^{(2)} = 4.89$ eV and $\hbar\gamma^{(2)}(T = 300 \text{ K}) = 0.0436$ eV for Ni [14, 82, 83]. For Ni-Ni plates $\hbar\omega_p^{(1)} = \hbar\omega_p^{(2)} = 4.89$ eV and $\hbar\gamma^{(1)}(T = 300 \text{ K}) = \hbar\gamma^{(2)}(T = 300 \text{ K}) = 0.0436$ eV.

To perform computations by Eqs. (2)–(5), one also needs information about the magnetic permeability at the pure imaginary Matsubara frequencies. Nickel falls into the category of soft ferromagnets which do not possess the spontaneous magnetization. Keeping in mind that the Casimir force is determined by the fluctuating electromagnetic field which exhibits the zero mean magnetic field, here we consider what is called the initial permeability corresponding to $\mathbf{H} = 0$.

The static value of this permeability, $\mu^{\text{Ni}}(0)$, is preserved up to the frequency $\omega_1 \approx 2\pi \times 10^5$ rad/s and becomes equal to unity in the region $\omega > \omega_2 \approx 6\pi \times 10^9$ rad/s (see Figure 14 in Ref. [84] using the data of Refs. [85–87]). Note that the first Matsubara frequency at $T = 300$ K is $\xi_1 \sim 10^{14}$ rad/s, i.e., much larger than the frequency ω_2 where the magnetic permeability of Ni drops to unity. Taking into account that the same situation holds for all ferromagnetic materials, it was concluded [88] that the magnetic properties can influence the Casimir force only through the zero-frequency term of the Lifshitz formula (2). Taking into account that the value of the static permeability of Ni is sample-dependent [89], below we use the value $\mu^{\text{Ni}}(0) = 110$ as for the samples used in the experiments [77–79] on measuring the Casimir force with magnetic surfaces. We recall that for the Au-Ni plates $\mu^{(1)}(i\xi_l) = 1$, $\mu^{(2)}(i\xi_l) = \mu^{\text{Ni}}(i\xi_l)$ and for the Ni-Ni plates $\mu^{(1)}(i\xi_l) = \mu^{(2)}(i\xi_l) = \mu^{\text{Ni}}(i\xi_l)$ where $\mu^{\text{Ni}}(i\xi_l)$ is

$$\mu^{\text{Ni}}(i\xi_l) = \begin{cases} \mu^{\text{Ni}}(0), & l = 0, \\ 1, & l \geq 1. \end{cases} \quad (7)$$

In Figure 1a, we present the computational results for the total Casimir forces per unit area computed by Eqs. (1)–(5) in the configuration of Au-Ni plates using the Drude and the plasma models as the functions of separation between plates. For the sake of convenience in presentation, these results are normalized to the high-temperature (large separation) limiting case of the Casimir force between the Au-Ni plates computed by means of the Drude model

$$F_D^0(a, T) = -\frac{k_B T}{4\pi a^3} \zeta(3), \quad (8)$$

where $\zeta(z)$ is the Riemann zeta function. This is equivalent to one half of the result for two ideal metal planes [13]. The upper line is computed using the plasma model and the lower line — by the Drude one. It is seen that there is a significant deviation between these two theoretical predictions.

Next, using Eqs. (2)–(5), we computed the contributions to the total Casimir force between the Au-Ni plates given by the electromagnetic waves with the TM and TE polarizations. The computational results for F_{TM} and F_{TE} obtained using the Drude and plasma models normalized to F_D^0 are shown in Figure 1b as the functions of separation. The upper line demonstrates the TM contribution to the total Casimir force which is essentially independent of the used model of the dielectric permittivity. Note that the TM contribution to the Casimir force does not depend on the magnetic properties because the TM reflection coefficient at zero Matsubara frequency $r_{\text{TM}}(0, k_{\perp}) = 1$. By contrast, the TE contributions to the Casimir force computed using the Drude model (the lower line) and the plasma model (the upper line) essentially depend on the model used. As is seen in Figure 1b, just the contributions of the TE polarizations computed using the two models determine the entire difference in the total Casimir forces shown in Figure 1a.

Similar results were obtained for the configuration of two magnetic Ni-Ni plates. In Figure 2a, the computational results for the total Casimir force per unit area found using the Drude and plasma models are shown as the functions of separation between the plates. As in Figure 1, these results are normalized to the values of F_D^0 defined in Eq. (8). According to Figure 2a, for two magnetic metals the theoretical predictions obtained using the Drude and plasma models are more different at short separations and less different at large separations than for one nonmagnetic and one magnetic metals. What is more, for two magnetic metals the predictions of these models interchange their places.

In Figure 2b, we present the computational results for F_{TM} and F_{TE} normalized to F_D^0 , which are obtained using the Drude and plasma models as the functions of separation in the configuration of Ni-Ni plates. The upper line shows the TM contribution

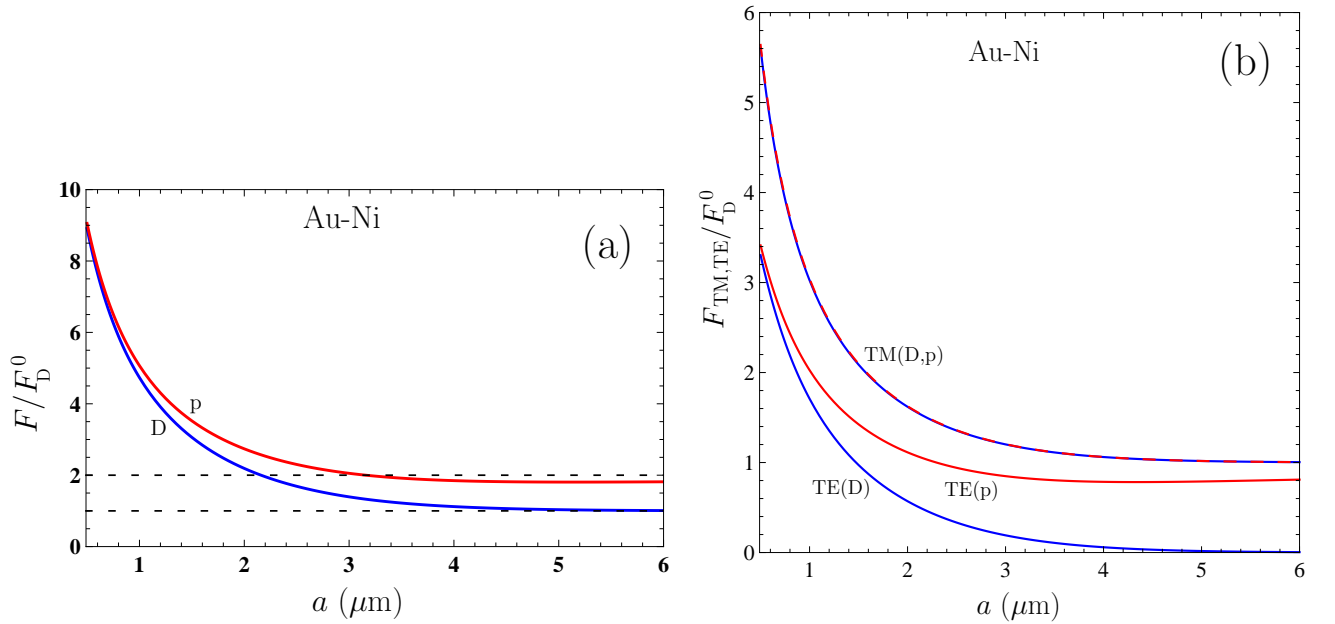


FIG. 1: (a) The Casimir forces per unit area and (b) the transverse magnetic (TM) and transverse electric (TE) contributions to the Casimir force computed using the Drude (D) and plasma (p) models in the configuration of Au-Ni plates and normalized to the high-temperature Casimir force found using the Drude model are shown as the functions of separation.

to the total Casimir force in this configuration which is again essentially independent of the used permittivity model. The TM contribution is also independent of the magnetic properties of Ni for the reason indicated above. The lower and medium lines show the contributions of the TE polarization computed using the Drude and plasma models, respectively. As is seen in Figure 2b, these predictions differ widely at both small and large separations. The difference between them fully determines the difference between the total Casimir forces computed by means of the Drude and plasma models in Figure 2a.

According to the above results, the Casimir puzzle for magnetic materials (similar to nonmagnetic ones [69]) is caused by the contribution of electromagnetic waves with the transverse electric polarization. As to the contribution of TM polarized electromagnetic waves, it can be safely computed using the Drude model with no contradiction with the measurement data. In

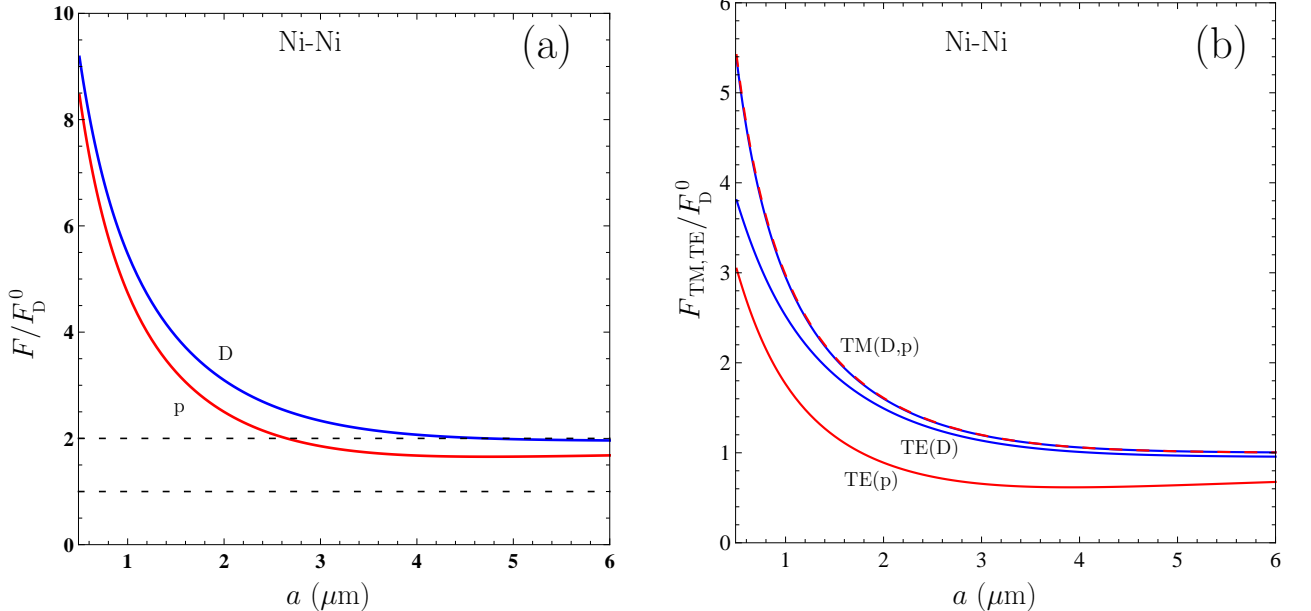


FIG. 2: (a) The Casimir forces per unit area and (b) the transverse magnetic (TM) and transverse electric (TE) contributions to the Casimir force computed using the Drude (D) and plasma (p) models in the configuration of Ni-Ni plates and normalized to the high-temperature Casimir force found using the Drude model are shown as the functions of separation.

order to further bring under control the roots of the Casimir puzzle for magnetic materials, it is important also to find out what fractions of the Casimir force in each of the TM and TE contributions are determined by the propagating and evanescent waves. To accomplish this, it is necessary to use the formulation of the Lifshitz theory along the real frequency axis.

III. THE LIFSHITZ FORMULA IN TERMS OF REAL FREQUENCIES FOR AU-NI AND NI-NI PLATES: PROPAGATING AND EVANESCENT WAVES

The Casimir force per unit area of two parallel plates is again represented by Eq. (1) as the sum of the transverse magnetic and transverse electric contributions. Each of these contributions is now expressed, although mathematically equivalent to Eq. (2), but quite differently as a sum of fractions determined by the propagating and evanescent waves

$$F_{\text{TM}}(a, T) = F_{\text{TM}}^{\text{prop}}(a, T) + F_{\text{TM}}^{\text{evan}}(a, T), \quad F_{\text{TE}}(a, T) = F_{\text{TE}}^{\text{prop}}(a, T) + F_{\text{TE}}^{\text{evan}}(a, T), \quad (9)$$

where [13]

$$F_{\text{TM,TE}}^{\text{prop}}(a, T) = -\frac{\hbar}{2\pi^2} \int_0^\infty d\omega \coth \frac{\hbar\omega}{2k_B T} \int_0^{\omega/c} k_\perp dk_\perp \text{Im} \left[q \frac{r_{\text{TM,TE}}^{(1)}(\omega, k_\perp) r_{\text{TM,TE}}^{(2)}(\omega, k_\perp) e^{-2aq}}{1 - r_{\text{TM,TE}}^{(1)}(\omega, k_\perp) r_{\text{TM,TE}}^{(2)}(\omega, k_\perp) e^{-2aq}} \right], \quad (10)$$

and

$$F_{\text{TM,TE}}^{\text{evan}}(a, T) = -\frac{\hbar}{2\pi^2} \int_0^\infty d\omega \coth \frac{\hbar\omega}{2k_B T} \int_{\omega/c}^\infty k_\perp dk_\perp q \text{Im} \frac{r_{\text{TM,TE}}^{(1)}(\omega, k_\perp) r_{\text{TM,TE}}^{(2)}(\omega, k_\perp) e^{-2aq}}{1 - r_{\text{TM,TE}}^{(1)}(\omega, k_\perp) r_{\text{TM,TE}}^{(2)}(\omega, k_\perp) e^{-2aq}}. \quad (11)$$

The reflection coefficients in Eqs. (10) and (11) are similar to Eq. (4) but depend on real frequencies ω :

$$r_{\text{TM}}^{(m)}(\omega, k_\perp) = \frac{\varepsilon^{(m)}(\omega)q - p^{(m)}}{\varepsilon^{(m)}(\omega)q + p^{(m)}}, \quad r_{\text{TE}}^{(m)}(\omega, k_\perp) = \frac{\mu^{(m)}(\omega)q - p^{(m)}}{\mu^{(m)}(\omega)q + p^{(m)}}, \quad (12)$$

where now

$$q = \left(k_\perp^2 - \frac{\omega^2}{c^2} \right)^{1/2}, \quad p^{(m)} = \left[k_\perp^2 - \varepsilon^{(m)}(\omega)\mu^{(m)}(\omega)\frac{\omega^2}{c^2} \right]^{1/2}. \quad (13)$$

The main feature of the propagating electromagnetic waves, which determine the fraction $F_{\text{TM,TE}}^{\text{prop}}$ in Eq. (10), is that $k_\perp = (k_1^2 + k_2^2)^{1/2} \leq \omega/c$, i.e., the mass-shell equation $k_\perp^2 + k_3^2 = \omega^2/c^2$, following from the wave equation, is satisfied with some real component of the wave vector k_3 (we assume that the Casimir plates are in the plane xy and the z axis is perpendicular to it). For the evanescent waves, which determine the fraction $F_{\text{TM,TE}}^{\text{evan}}$ in Eq. (11), contrastingly, it holds $k_\perp > \omega/c$, i.e., the mass-shell equation is satisfied with only the pure imaginary $k_3 = iq$. This leads to the exponentially fast decay, $\sim \exp(ik_3z) = \exp(-qz)$, of the evanescent waves in the direction perpendicular to the plate explaining another name, "the surface waves", for this physical phenomenon.

Equations (9)–(11) are inconvenient for using in numerical computations of the Casimir force. The problem is that the fraction of the propagating waves in Eq. (10), in accordance with Eq. (13), contains the exponent of pure imaginary power $-2aq$, which necessitates to calculate the integrals of the quickly oscillating functions (see, e.g., Ref. [90]). At the same time, for the fractions of the evanescent waves in Eq. (11), the quantity q is real which ensures against quick oscillations of the integrands and makes possible the numerical integration.

In order to perform computations of the fractions of evanescent and propagating waves (10) and (11), one needs the dielectric permittivities of Au and Ni plates and the magnetic permeability of the Ni plate along the real frequency axis. Thus, the dielectric permittivities of the Drude and plasma models are given by

$$\varepsilon_{\text{D}}^{(m)}(\omega) = 1 - \frac{(\omega_p^{(m)})^2}{\omega[\omega + i\gamma^{(m)}(T)]}, \quad \varepsilon_{\text{p}}^{(m)}(\omega) = 1 - \frac{(\omega_p^{(m)})^2}{\omega^2}, \quad (14)$$

where the values of the plasma frequencies and relaxation parameters for Au and Ni were indicated in Section 2.

In Figure 3, the magnitude of the real part of dielectric permittivity of the Drude model (a) and its imaginary part (b) are shown by the upper and lower solid lines for Au and Ni plates, respectively. The upper and lower dashed lines in Figure 3a show the magnitude of dielectric permittivity of the plasma model, which is real, for Au and Ni plates, respectively. Figures 3a and 3b

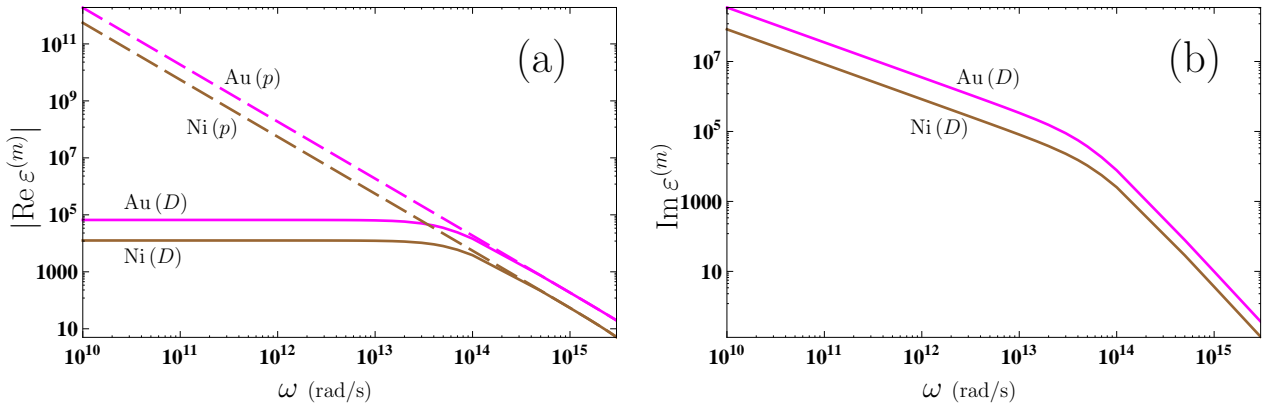


FIG. 3: (a) The magnitudes of real parts of the dielectric permittivities of the Drude and plasma models and (b) the imaginary parts of the dielectric permittivity of the Drude model are shown by the pairs of solid (the Drude model) and dashed (the plasma model) lines as the functions of frequency. In all cases the upper and lower lines in each pair are plotted for Au and Ni plates, respectively.

are plotted up to the largest frequencies contributing to the computational results over the region of chosen separations from 0.5 to 6 μm . The plotted straight lines can be extrapolated to the frequencies below 10^{10} rad/s contributing to the Casimir force.

As discussed in Section 2, when using the Lifshitz formula for magnetic materials written in terms of Matsubara frequencies, at not too low temperature one needs to know only the value of the static magnetic permeability. However, the computations of the Casimir force using Eqs. (10)–(13) written in terms of real frequencies require the knowledge of magnetic permeability over the wide frequency region. According to discussion in Section 2, the static magnetic permeability of Ni sample under consideration $\mu(0) = 110$ preserves its value up to the frequency $\omega_1 \approx 2\pi \times 10^5$ rad/s and is equal to unity in the region $\omega > \omega_2 \approx 6\pi \times 10^9$ rad/s [83–86]. Within the frequency region (ω_1, ω_2) , where the magnetic permeability of Ni essentially depends on the frequency, it can be approximately described by the Debye model [83]. Combining these pieces of information, the magnetic permeability of Ni over the entire axis of real frequencies can be represented as

$$\mu^{(m)}(\omega) = \begin{cases} \mu^{\text{Ni}}(0), & 0 \leq \omega \leq \omega_1, \\ 1 + \frac{\mu^{\text{Ni}}(0)-1}{1-i\omega/\omega_{ch}}, & \omega_1 < \omega \leq \omega_2, \\ 1, & \omega > \omega_2, \end{cases} \quad (15)$$

where the characteristic frequency $\omega_{ch} \approx 2\pi \times 10^7$ rad/s is obtained using Figure 14 in Ref. [84]. Note that the computational results presented below do not depend on variations in the value of ω_{ch} if the values of ω_1 and ω_2 remain unchanged.

In Figure 4, the real (a) and imaginary (b) parts of the magnetic permeability (15) are shown as the functions of frequency. In the next two sections, the data of Figures 3 and 4 are used for computations of the fractions of evanescent and propagating waves in the transverse magnetic and transverse electric contributions to the Casimir force.

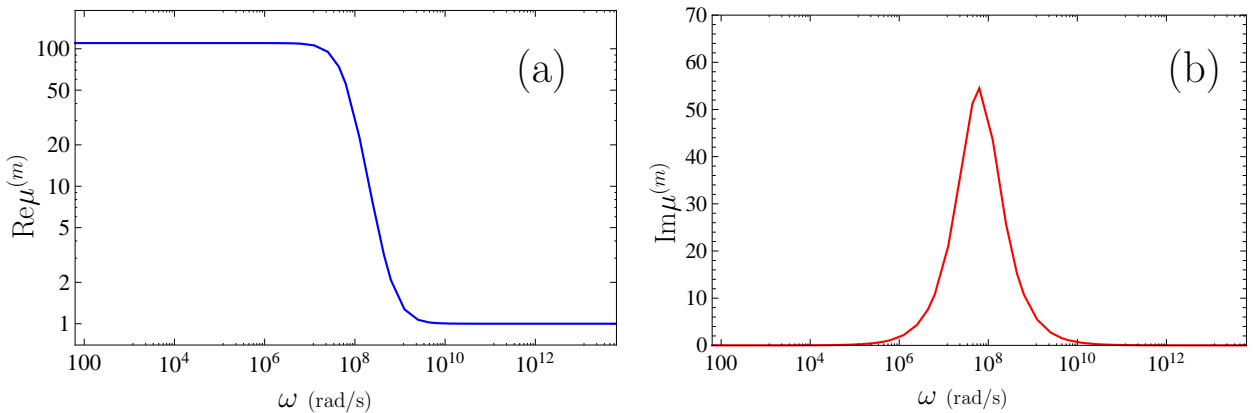


FIG. 4: (a) The real and (b) imaginary parts of the magnetic permeability of Ni are shown as the functions of frequency.

IV. FRACTIONS DUE TO EVANESCENT AND PROPAGATING WAVES IN THE TRANSVERSE MAGNETIC CONTRIBUTIONS TO THE CASIMIR FORCE FOR AU-NI AND NI-NI PLATES IN THE FORMALISM OF REAL FREQUENCIES

We start from the computation of the fraction of evanescent waves (11) in the transverse magnetic contribution to the Casimir force F_{TM} defined in Eq. (2). It is convenient to perform numerical computations by Eq. (11) using, instead of the dimensional variables ω and k_{\perp} , the dimensionless ones defined as

$$t = \frac{\omega}{\omega_c} \equiv \frac{2a}{c}\omega, \quad w = 2ak_{\perp} - t. \quad (16)$$

In terms of these variables, the fraction of evanescent waves (11) in the TM contribution to the Casimir force takes the form

$$F_{\text{TM}}^{\text{evan}}(a, T) = -\frac{\hbar c}{32\pi^2 a^4} \int_0^{\infty} dt \coth\left(\frac{\hbar c}{4ak_B T}t\right) \int_0^{\infty} dw (w+t) \sqrt{w^2 + 2wt} \text{Im} \frac{r_{\text{TM}}^{(1)}(t, w) r_{\text{TM}}^{(2)}(t, w) e^{-\sqrt{w^2 + 2wt}}}{1 - r_{\text{TM}}^{(1)}(t, w) r_{\text{TM}}^{(2)}(t, w) e^{-\sqrt{w^2 + 2wt}}}. \quad (17)$$

Here, the reflection coefficient expressed via the variables (16) is given by

$$r_{\text{TM}}^{(m)}(t, w) = \frac{\varepsilon^{(m)}(\omega_c t) \sqrt{w^2 + 2wt} - \sqrt{(w+t)^2 - \varepsilon^{(m)}(\omega_c t) \mu^{(m)}(\omega_c t) t^2}}{\varepsilon^{(m)}(\omega_c t) \sqrt{w^2 + 2wt} + \sqrt{(w+t)^2 - \varepsilon^{(m)}(\omega_c t) \mu^{(m)}(\omega_c t) t^2}}. \quad (18)$$

The dielectric permittivities (14) entering Eq. (18) are expressed as

$$\varepsilon_{\text{D}}^{(m)}(\omega_c t) = 1 - \frac{(\tilde{\omega}_p^{(m)})^2}{t[t + i\tilde{\gamma}^{(m)}(T)]}, \quad \varepsilon_{\text{p}}^{(m)}(\omega_c t) = 1 - \frac{(\tilde{\omega}_p^{(m)})^2}{t^2}, \quad (19)$$

where $\tilde{\omega}_p^2 = \omega_p^2/\omega_c^2$ and $\tilde{\gamma}^{(m)} = \gamma^{(m)}/\omega_c$, and the magnetic permeability of Ni (15) is

$$\mu^{(m)}(\omega_c t) = \begin{cases} \mu^{\text{Ni}}(0), & 0 \leq t \leq \frac{\omega_1}{\omega_c}, \\ 1 + \frac{\mu^{\text{Ni}}(0)-1}{1-i\omega_c t/\omega_{ch}}, & \frac{\omega_1}{\omega_c} < t \leq \frac{\omega_2}{\omega_c}, \\ 1, & t > \frac{\omega_2}{\omega_c}, \end{cases} \quad (20)$$

As discussed in Section 3, computations of the fraction of propagating waves (10) in the TM contribution to the Casimir force is made difficult due to a presence of the rapidly oscillating function under the integral. This fraction can, however, be found in a simpler way using the full contribution of the transverse magnetic polarization F_{TM} found in Section 2 using the Lifshitz formula written in terms of imaginary Matsubara frequencies

$$F_{\text{TM}}^{\text{prop}}(a, T) = F_{\text{TM}}(a, T) - F_{\text{TM}}^{\text{evan}}(a, T). \quad (21)$$

In Figure 5, the lower and upper dashed lines present the computational results normalized to F_{D}^0 for the fractions of evanescent and propagating waves in F_{TM} computed in the configuration of Au-Ni plates using the Drude model by Eqs. (17)–(20) and (21), respectively. The integration in Eq. (17) was performed using the adaptive Gauss-Kronrod quadrature method. It was checked that the obtained results are stable with respect to changing the number of nodes. For comparison purposes, the solid line reproduced from Figure 1b shows the total transverse magnetic contribution $F_{\text{TM(D)}}$. As is seen in Figure 5, the contribution of the propagating waves to the Casimir force is negative [we recall that F_{D}^0 defined in Eq. (8) is also negative], which corresponds to attraction, whereas the contribution of the evanescent waves is positive, which corresponds to repulsion. Taking into account that $|F_{\text{TM(D)}}^{\text{prop}}| > |F_{\text{TM(D)}}^{\text{evan}}|$, one obtains the attractive TM contribution to the Casimir force $F_{\text{TM(D)}}$ shown by the solid line in Figure 5. Note that the fractions of evanescent and propagating waves in F_{TM} essentially do not depend on the magnetic properties as in the case with the total F_{TM} .

For the plasma model, the dielectric permittivity is real, whereas the imaginary part of the magnetic permeability of Ni results in only a negligibly small contribution to $F_{\text{TM}}^{\text{evan}}$. As a result, if the plasma model is used in computations, one obtains to a high degree of precision

$$F_{\text{TM(p)}}^{\text{evan}}(a, T) = 0, \quad F_{\text{TM(p)}}^{\text{prop}}(a, T) = F_{\text{TM(p)}}(a, T). \quad (22)$$

Similar computations have been performed for the configuration of Ni-Ni plates using the Drude model. The computational results, which differ from the case of Au-Ni plates only quantitatively, are shown in Figure 6. The lower and upper dashed lines demonstrate the fractions of evanescent and propagating waves in $F_{\text{TM(D)}}$ computed using Eqs. (17)–(20) and (21), respectively.

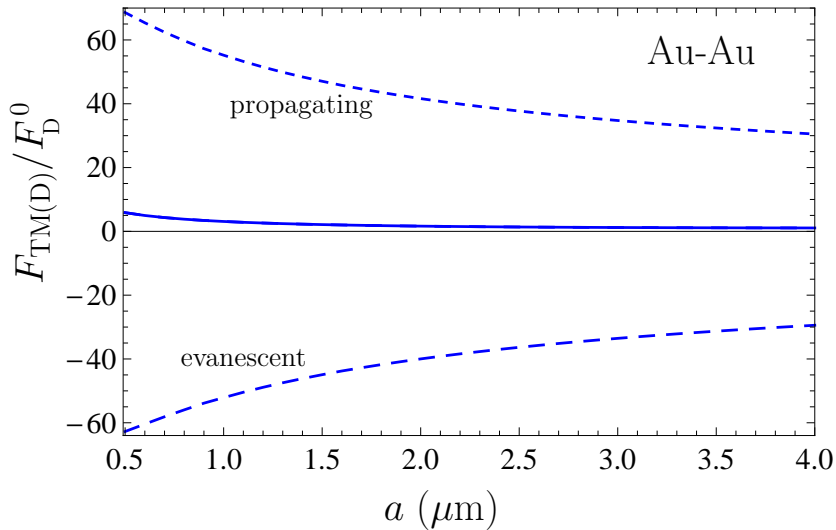


FIG. 5: The fractions of the evanescent and propagating waves in the transverse magnetic contribution to the Casimir force per unit area of Au-Ni plates computed using the Drude model are shown by the lower and upper dashed lines as the functions of separation. The total transverse magnetic contribution to the Casimir force computed by the Drude model shown by the solid line is reproduced from Figure 1b.

The propagating waves again correspond to the Casimir attraction and the evanescent waves — to a repulsion. Their sum in accordance with Eq. (9) results in a smaller magnitude attractive TM contribution to the Casimir force $F_{\text{TM(D)}}$ shown in Figure 6 by the solid line. If the plasma model is used in computations of the fractions of evanescent and propagating waves in F_{TM} for Ni-Ni plates, one again arrives to Eq. (22), i.e., to a high degree of precision, the evanescent waves do not contribute to the transverse magnetic part of the Casimir force F_{TM} .

Thus, although the transverse magnetic contribution to the Casimir force with magnetic materials does not depend on whether the Drude or the plasma model is used in computations, the fractions of evanescent and propagating waves in these contributions heavily depend on the used permittivity model. Similar situation was revealed earlier for the case of Casimir force between the nonmagnetic Au-Au plates [69]. Note, however, that due to an error in the computer program the magnitudes of the fractions of evanescent and propagating waves contributing to $F_{\text{TM(D)}}$ in Figure 4 of Ref. [69] are shown with much smaller magnitudes than they really have. The correct fractions of the evanescent and propagating waves in the transverse magnetic contribution to the Casimir force for Au-Au plates computed by Eqs. (17)–(21) with $\epsilon_{\text{D}}^{(1)}(\omega_c t) = \epsilon_{\text{D}}^{(2)}(\omega_c t) = \epsilon_{\text{D}}^{\text{Au}}(\omega_c t)$ are shown in Figure 7 by

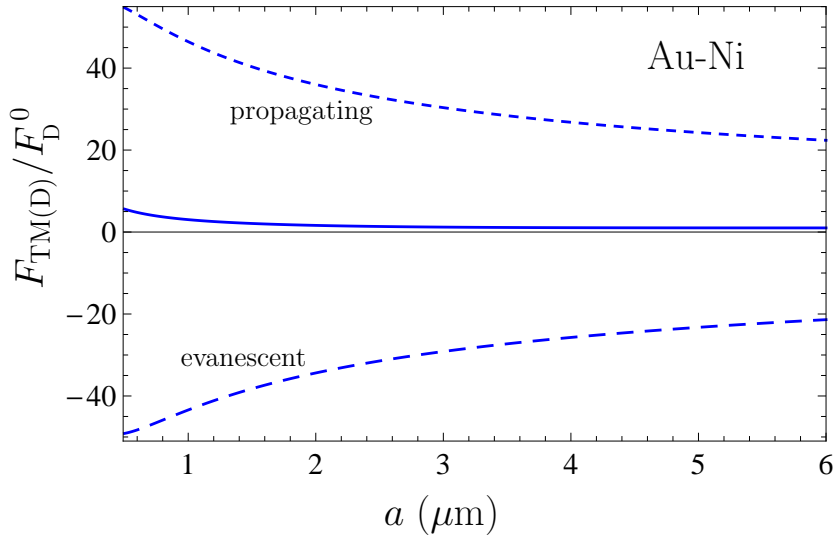


FIG. 6: The fractions of the evanescent and propagating waves in the transverse magnetic contribution to the Casimir force per unit area of Ni-Ni plates computed using the Drude model are shown by the lower and upper dashed lines as the functions of separation. The total transverse magnetic contribution to the Casimir force computed by the Drude model shown by the solid line is reproduced from Figure 2b.

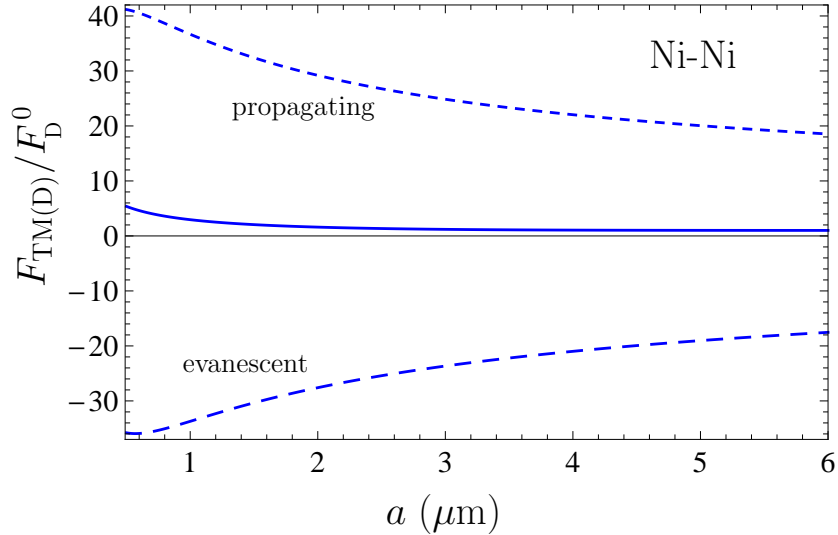


FIG. 7: The fractions of the evanescent and propagating waves in the transverse magnetic contribution to the Casimir force per unit area of Au-Au plates computed using the Drude model are shown by the lower and upper dashed lines as the functions of separation.

the lower and upper dashed lines as the functions of separation. The solid line indicates the total TM contribution $F_{\text{TM}(D)}$ to the Casimir force coinciding with that shown in Figure 4 of Ref. [69].

V. FRACTIONS DUE TO EVANESCENT AND PROPAGATING WAVES IN THE TRANSVERSE ELECTRIC CONTRIBUTIONS TO THE CASIMIR FORCE FOR AU-NI AND NI-NI PLATES IN THE FORMALISM OF REAL FREQUENCIES

We are coming now to the constituent parts of the transverse electric contribution to the Casimir force with magnetic plates which are of major importance in the context of the Casimir puzzle. In terms of the dimensionless variables (16), the fraction of evanescent waves in the TE contribution (11) is expressed similar to Eq. (17)

$$F_{\text{TE}}^{\text{evan}}(a, T) = -\frac{\hbar c}{32\pi^2 a^4} \int_0^\infty dt \coth\left(\frac{\hbar c}{4a k_B T} t\right) \int_0^\infty dw (w+t) \sqrt{w^2 + 2wt} \text{Im} \frac{r_{\text{TE}}^{(1)}(t, w) r_{\text{TE}}^{(2)}(t, w) e^{-\sqrt{w^2 + 2wt}}}{1 - r_{\text{TE}}^{(1)}(t, w) r_{\text{TE}}^{(2)}(t, w) e^{-\sqrt{w^2 + 2wt}}}. \quad (23)$$

The TE reflection coefficient expressed via the variables (16) is given by

$$r_{\text{TE}}^{(m)}(t, w) = \frac{\mu^{(m)}(\omega_c t) \sqrt{w^2 + 2wt} - \sqrt{(w+t)^2 - \varepsilon^{(m)}(\omega_c t) \mu^{(m)}(\omega_c t) t^2}}{\mu^{(m)}(\omega_c t) \sqrt{w^2 + 2wt} + \sqrt{(w+t)^2 - \varepsilon^{(m)}(\omega_c t) \mu^{(m)}(\omega_c t) t^2}}, \quad (24)$$

where the dielectric permittivities and magnetic permeability are given by Eqs. (19) and (20).

In order to avoid a challenging task of integration the rapidly oscillating functions in Eq. (10), the fraction of the propagating waves is found from

$$F_{\text{TE}}^{\text{prop}}(a, T) = F_{\text{TE}}(a, T) - F_{\text{TE}}^{\text{evan}}(a, T), \quad (25)$$

where F_{TE} is computed in Section 2 using the formalism of pure imaginary Matsubara frequencies.

The computational results for the fractions of evanescent and propagating waves obtained by Eqs. (23)–(25) using the Drude model by means of the adaptive Gauss-Kronrod quadrature method for the case of Au-Ni plates normalized to F_D^0 are shown by the lower and upper dashed lines in Figure 8 as the functions of separation. The solid line reproduced from Figure 1b for comparison purposes shows the total transverse electric contribution to the Casimir force for Au-Ni plates computed using the Drude model. As is seen in Figure 8, the propagating waves are again responsible for attraction and the evanescent ones for repulsion. Taking into account that the attractive part is larger in magnitude, the total transverse electric contribution is attractive similar to the transverse magnetic one (see the solid line in Figure 8). According to our computational results, the fraction of evanescent waves $F_{\text{TE}(D)}^{\text{evan}}$ does not depend on magnetic properties to a high degree of precision.

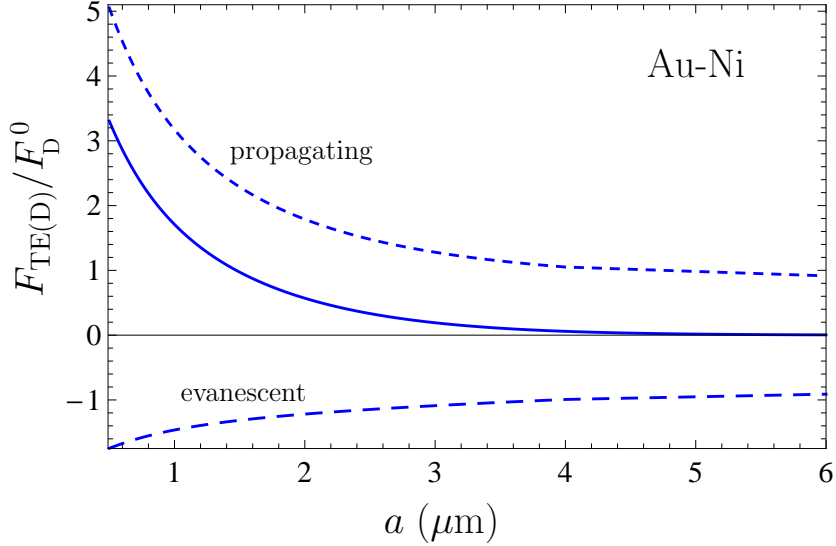


FIG. 8: The fractions of the evanescent and propagating waves in the transverse electric contribution to the Casimir force per unit area of Au-Ni plates computed using the Drude model are shown by the lower and upper dashed lines as the functions of separation. The total transverse electric contribution to the Casimir force computed by the Drude model shown by the solid line is reproduced from Figure 1b.

Now, computations of the fractions of evanescent and propagating waves in the transverse electric contribution to the Casimir force for Au-Ni plates by Eqs. (23)–(25) are performed using the plasma model. The imaginary part of the magnetic permeability (20) leads to a negligibly small contribution to $F_{\text{TE(p)}}^{\text{evan}}$. As a result, from Eq. (25) we have

$$F_{\text{TE(p)}}^{\text{evan}}(a, T) = 0, \quad F_{\text{TE(p)}}^{\text{prop}}(a, T) = F_{\text{TE(p)}}(a, T). \quad (26)$$

Thus, $F_{\text{TE(p)}}^{\text{evan}}$ also does not depend on the magnetic properties of Ni. In fact for Au-Ni plates the Casimir force depends on magnetic properties only if the plasma model is used in computations and this dependence is contained in $F_{\text{TE(p)}}^{\text{prop}}$.

Computation of the fractions of evanescent and propagating waves by Eqs. (23)–(25) using the Drude and plasma models was also performed for the case of Ni-Ni plates. The computational results using the Drude model normalized to F_D^0 are shown in Figure 9 where the lower and upper dashed lines show the fractions of evanescent and propagating waves, respectively, whereas the solid line reproduced from Figure 2b represents the total transverse electric contribution. Its part determined by the propagating waves is larger in magnitude, so that the transverse electric contribution to the force is attractive. Similar to the case of Au-Ni plates, for Ni-Ni plates $F_{\text{TE(D)}}^{\text{evan}}$ is practically independent of magnetic properties.

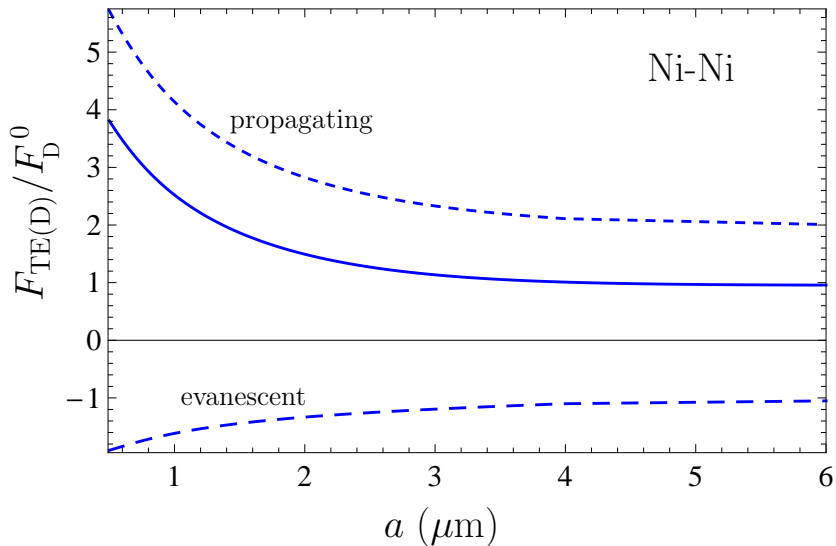


FIG. 9: The fractions of the evanescent and propagating waves in the transverse electric contribution to the Casimir force per unit area of Ni-Ni plates computed using the Drude model are shown by the lower and upper dashed lines as the functions of separation. The total transverse electric contribution to the Casimir force computed by the Drude model shown by the solid line is reproduced from Figure 2b.

If the plasma model is used in computations for the case of Ni-Ni plates, one again arrives at Eq. (26), i.e., to the fact that the fraction of evanescent waves $F_{TE(p)}^{evan}$ is negligibly small. Similar to the case of Au-Ni plates, for Ni-Ni plates $F_{TE(D,p)}^{evan}$ are practically independent on magnetic properties. The dependence of magnetic properties is contained in F_{TE}^{prop} irrespective of whether the Drude or the plasma model is used.

From the above results, it is seen that there are both similarities and distinctions between the cases of nonmagnetic and magnetic metals as to the origin of the Casimir puzzle. According to Section 1, for nonmagnetic metals the difference in theoretical Casimir forces calculated using the Drude and plasma models is due to the fraction of transverse electric evanescent waves. In doing so, the total contribution of transverse magnetic waves and also the fraction of propagating waves in the contribution of transverse electric polarization to the Casimir force can be calculated using the Drude model with no contradiction with the measurement data. In a similar way, for magnetic metals, the total contribution of transverse magnetic polarization does not depend on whether the Drude or the plasma model is used.

However, as opposed to the case of nonmagnetic metals, for magnetic metals not only the fraction of evanescent waves, but also the fraction of propagating waves in the transverse electric contribution to the Casimir force as well depends on the model of dielectric permittivity used. To see this, one should compare the upper dashed line in Figure 8 representing $F_{TE(D)}^{prop}$ with the middle line in Figure 1b representing $F_{TE(p)} = F_{TE(p)}^{prop}$ for the Au-Ni plates and the upper dashed line in Figure 9 representing $F_{TE(D)}^{prop}$ with the bottom line in Figure 2b representing $F_{TE(p)} = F_{TE(p)}^{prop}$ for the Ni-Ni plates. From this it follows that for the Casimir force with magnetic plates a contradiction between computations by means of the Lifshitz theory using the Drude model and the measurement data is due to the contribution of transverse electric polarization.

It is worth noting that, according to the results of Section 2, the transverse magnetic contribution to the Casimir force between metallic plates does not depend on the value of magnetic permeability. In addition, as shown in this section, the fraction of evanescent waves in the transverse electric contribution to the Casimir force with magnetic plates also does not depend on the magnetic permeability with pinpoint accuracy for both the Drude and the plasma models. In doing so, $F_{TE(p)}^{evan} = 0$ to a high precision whereas $F_{TE(D)}^{evan}$, although is not equal to zero, is independent of μ . An independence on μ in the above mentioned cases arises due to the fact that μ is not equal to unity only in the frequency region lying much below the characteristic interval around the frequency $c/(2a)$ giving the major contribution to the Casimir force. Thus, an impact of magnetic properties on the Casimir force between metallic plates is determined by only a fraction of the propagating waves in the transverse electric contribution.

VI. DISCUSSION

The Casimir force in configurations with magnetic plates considered in this article is the subject of prime importance because in this case a comparison between experiment and theory provides the most convincing and unambiguous evidence concerning the Casimir puzzle and places strong constraints on the ways of its resolution. As discussed in Section 1, for the case of nonmagnetic plates the Casimir puzzle is due to a contribution of transverse electric evanescent waves which is incorrectly described by the Drude model. The inadequacy of the Drude model in this case was directly demonstrated in the independent experiment [76] related to classical electrodynamics. The use of the plasma model leads to even greater disagreement with this experiment. The reason is that the characteristic values of the parameter ck_{\perp}/ω in the experimental configuration of Ref. [76] and in measurements of the Casimir force differ by 5 orders of magnitude.

According to the above results, for the Casimir force with magnetic plates the situation is more complicated. We have shown that in this case the difference in theoretical predictions of the Lifshitz theory using the Drude and plasma models resulting in contradiction with the measurement data originates from the transverse electric contribution given by both the evanescent and propagating waves. In doing so, only a fraction of the propagating waves with the transverse electric polarization depends on the magnetic properties of the plates. This raises a question of whether one could doubt in the applicability of the Drude model to magnetic plates not only in the region of the TE evanescent, but TE propagating waves as well.

When answering this question positively, it should be remembered that the Drude model was originally created for the case of nonmagnetic metals and it is not directly applicable to the ferromagnetic materials (see both the theoretical and experimental results on this subject in Refs. [91–97]). Unlike the case of nonmagnetic metals, the Drude model fails to correctly describe the electric conductivity even in the region of propagating waves. This affects the low-frequency behavior of the TE reflection coefficient. Calculations show that when the Casimir force with magnetic plates is computed using the Drude model the contribution of TE polarized propagating waves, which depends on the magnetic permeability, is much larger than in the case when the plasma model is used in computations. The discussed problems make it necessary to search for a more adequate response functions of nonmagnetic materials in the region of transverse electric evanescent waves and of magnetic materials for both the evanescent and propagating waves with the transverse electric polarization.

An experience of graphene, where the response functions are found starting from the first principles of thermal quantum field theory, suggests that a generalization of the dielectric permittivity of the Drude model should be spatially nonlocal and possess the double pole at zero frequency [98, 99]. The phenomenological examples of the permittivities of such kind were considered

for both nonmagnetic [100] and magnetic [101] metals. These permittivities bring the predictions of the Lifshitz theory in agreement with the measurement data of all performed experiments on measuring the Casimir force [102] but are lacking the necessary fundamental justification. There are also other nonlocal generalizations of the Drude model motivated by the Casimir puzzle [20, 103, 104], but the Lifshitz theory using these generalizations is not consistent with experiment.

It would be interesting to directly check the Drude model for magnetic materials in the region of transverse electric propagating waves in an experiment similar to that proposed in Refs. [67, 68] for the case of nonmagnetic metals and already performed in Ref. [76] confirming a violation of the Drude model in the region of TE evanescent waves. The realization of such an experiment would finally give an insight into the roots of the Casimir puzzle for magnetic materials.

VII. CONCLUSIONS

In the foregoing, we investigated the reasons of disagreement between the predictions of the Lifshitz theory for the Casimir force between Au-Ni and Ni-Ni plates obtained using the Drude model and the measurement data of several high-precision experiments. For this purpose, we have computed not only the total Casimir force in the mentioned configurations and the contributions to it given by the electromagnetic waves with the TM and TE polarizations, but also the fractions of each of these contributions given by the evanescent and propagating waves. All computations were performed using the dielectric permittivities of the Drude and plasma models and the magnetic permeability of Ni given by the Debye model in the separation region from 0.5 to 6 μm , where the response of metals to the electromagnetic field is fully determined by conduction electrons.

According to our results, the predictions of the Lifshitz theory for the transverse magnetic contributions to the Casimir force for both Au-Ni and Ni-Ni plates do not depend on whether the Drude or the plasma model is used in computations. On the contrary, the transverse electric contribution to the force was found to be highly dependent on the used model of dielectric permittivity. Just a difference between the values of the transverse electric contribution computed using the Drude model and the experimentally consistent plasma model determines a discrepancy between the predicted and experimental values of the Casimir force. At the same time, it was shown that the transverse magnetic contribution to the Casimir force does not depend on the magnetic permeability of the plates made of magnetic metal.

Using a formulation of the Lifshitz theory along the real frequency axis, we computed the fractions of the evanescent and propagating waves in both the transverse magnetic and transverse electric contributions to the Casimir force. It was shown that the propagating waves contribute to an attraction and the evanescent ones - to a repulsion resulting in total in the attractive Casimir force. Both the fractions of evanescent and propagating waves in the transverse electric contribution to the Casimir force were found dependent on a model of dielectric permittivity used. This is different from the case of nonmagnetic metals investigated earlier where only the fraction of evanescent waves in the transverse electric contribution to the Casimir force depends on whether the Drude or the plasma model is used in computations. On the other hand, it was shown that the impact of magnetic properties is caused by only a fraction of the propagating waves in the transverse electric contribution to the Casimir force.

To conclude, for magnetic metals the Drude model fails to precisely describe the electromagnetic response not only in the region of transverse electric evanescent waves (for nonmagnetic metals this was already independently confirmed experimentally), but in the region of transverse electric propagating waves as well. This allows to make primary emphasis upon the search for a more adequate theoretical description of the electromagnetic response of magnetic metals on the basis of first physical principles.

The work of G.L.K. and V.M.M. was partially supported by the State Assignment for Basic Research (project FSEG-2026-0018).

- [1] Heisenberg, W. Über quantentheoretische Umdeutung kinematischer und mechanischer Beziehungen. *Zeitschrift für Physik* **1925**, 33, 879–893.
- [2] Schrödinger, E. An Undulatory Theory of the Mechanics of Atoms and Molecules. *Phys. Rev.* **1926**, 28, 1049–1070.
- [3] Parsegian, V.A. *Van der Waals Forces: A Handbook for Biologists, Chemists, Engineers, and Physicists*; Cambridge University Press: Cambridge, UK, 2005.
- [4] London, F. Zur Theorie und Systematik der Molekularkräfte. *Z. Phys.* **1930**, 63, 245–279.
- [5] Casimir, H.B.G. On the attraction between two perfectly conducting plates. *Proc. K. Ned. Akad. Wet. B* **1948**, 51, 793–795.
- [6] Lifshitz, E.M. The theory of molecular attractive forces between solids. *Zh. Eksp. Teor. Fiz.* **1955**, 29, 94–110; Translated: *Sov. Phys. JETP* **1956**, 2, 73–83.
- [7] Dzyaloshinskii, I.E.; Lifshitz, E.M.; Pitaevskii, L.P. The general theory of van der Waals forces. *Usp. Fiz. Nauk* **1961**, 73, 381–422; Translated: *Adv. Phys.* **1961**, 10, 165–209.
- [8] Lifshitz, E.M.; Pitaevskii, L.P. *Statistical Physics, Part II*; Pergamon: Oxford, UK, 1980.

[9] Decca, R.S.; Fischbach, E.; Klimchitskaya, G.L.; Krause, D.E.; López, D.; Mostepanenko, V.M. Improved tests of extra-dimensional physics and thermal quantum field theory from new Casimir force measurements. *Phys. Rev. D* **2003**, *68*, 116003.

[10] Decca, R.S.; López, D.; Fischbach, E.; Klimchitskaya, G.L.; Krause, D.E.; Mostepanenko, V.M. Precise comparison of theory and new experiment for the Casimir force leads to stronger constraints on thermal quantum effects and long-range interactions. *Ann. Phys. (N.Y.)* **2005**, *318*, 37–80.

[11] Decca, R.S.; López, D.; Fischbach, E.; Klimchitskaya, G.L.; Krause, D.E.; Mostepanenko, V.M. Tests of new physics from precise measurements of the Casimir pressure between two gold-coated plates. *Phys. Rev. D* **2007**, *75*, 077101.

[12] Decca, R.S.; López, D.; Fischbach, E.; Klimchitskaya, G.L.; Krause, D.E.; Mostepanenko, V.M. Novel constraints on light elementary particles and extra-dimensional physics from the Casimir effect. *Eur. Phys. J. C* **2007**, *51*, 963–975.

[13] Bordag, M.; Klimchitskaya, G.L.; Mohideen, U.; Mostepanenko, V.M. *Advances in the Casimir Effect*; Oxford University Press: Oxford, UK, 2015.

[14] Palik, E.D. (Ed.) *Handbook of Optical Constants of Solids*; Academic Press: New York, USA, 1985.

[15] Klimchitskaya, G.L.; Mohideen, U.; Mostepanenko, V.M. The Casimir force between real materials: Experiment and theory. *Rev. Mod. Phys.* **2009**, *81*, 1827–1885.

[16] Høye, J.S.; Brevik, I.; Aarseth, J.B.; Milton, K.A. What is the temperature dependence of the Casimir effect? *J. Phys. A: Math. Gen.* **2006**, *39*, 6031–6038.

[17] Brevik, I.; Ellingsen, S.A.; Høye, J.S.; Milton, K.A. Analytical and numerical demonstration on how the Drude dispersive model satisfies Nernst's theorem for the Casimir entropy. *J. Phys. A: Math. Theor.* **2008**, *41*, 164017.

[18] Brevik, I.; Høye, J.S. Temperature dependence of the Casimir force. *Eur. J. Phys.* **2014**, *35*, 015012.

[19] Høye, J.S.; Brevik, I. Casimir force between a half-space and a plate of finite thickness. *Phys. Rev. A* **2016**, *93*, 052504.

[20] Brevik, I.; Shapiro, B. A critical discussion of different methods and models in Casimir effect. *J. Phys. Commun.* **2022**, *6*, 015005.

[21] Chang, C.-C.; Banishev, A.A.; Castillo-Garza, R.; Klimchitskaya, G.L.; Mostepanenko, V.M.; Mohideen, U. Gradient of the Casimir force between Au surfaces of a sphere and a plate measured using an atomic force microscope in a frequency-shift technique. *Phys. Rev. B* **2012**, *85*, 165443.

[22] Xu, J.; Klimchitskaya, G.L.; Mostepanenko, V.M.; Mohideen, U. Reducing detrimental electrostatic effects in Casimir-force measurements and Casimir-force-based microdevices. *Phys. Rev. A* **2018**, *97*, 032501.

[23] Liu, M.; Xu, J.; Klimchitskaya, G.L.; Mostepanenko, V.M.; Mohideen, U. Examining the Casimir puzzle with an upgraded AFM-based technique and advanced surface cleaning. *Phys. Rev. B* **2019**, *100*, 081406(R).

[24] Liu, M.; Xu, J.; Klimchitskaya, G.L.; Mostepanenko, V.M.; Mohideen, U. Precision measurements of the gradient of the Casimir force between ultraclean metallic surfaces at larger separations. *Phys. Rev. A* **2019**, *100*, 052511.

[25] Bimonte, G.; Spreng, B.; Maia Neto, P.A.; Ingold, G.-L.; Klimchitskaya, G.L.; Mostepanenko, V.M.; Decca, R.S. Measurement of the Casimir Force between 0.2 and 8 μm : Experimental Procedures and Comparison with Theory. *Universe* **2021**, *7*, 93.

[26] Klimchitskaya, G.L.; Mostepanenko, V.M. Experiment and theory in the Casimir effect. *Contemp. Phys.* **2006**, *47*, 131–144.

[27] Bimonte, G.; Emig, T.; Kardar, M.; Krüger, M. Nonequilibrium Fluctuational Quantum Electrodynamics: Heat Radiation, Heat Transfer, and Force. *Ann. Rev. Condens. Matter Phys.* **2017**, *8*, 119–143.

[28] Milton, K.A.; Li, Y.; Kalauni, P.; Parashar, P.; Guérout, P.; Ingold, G.-L.; Lambrecht, A.; Reynaud, S. Negative Entropies in Casimir and Casimir-Polder Interactions. *Fortschr. Phys.* **2017**, *65*, 1600047.

[29] Genet, C.; Lambrecht, A.; Maia Neto, P.; Reynaud, S. The Casimir force between rough metallic plates. *EPL* **2003**, *62*, 484–490.

[30] Maia Neto, P.A.; Lambrecht, A.; Reynaud, S. Casimir effect with rough metallic mirrors. *Phys. Rev. A* **2005**, *72*, 012115.

[31] Leskova, T.A.; Maradudin, A.A.; Munoz-Lopez, J. Coherence of light scattered from a randomly rough surface. *Phys. Rev. E* **2005**, *71*, 036606.

[32] van Zwol, P.J.; Palasantzas, G.; De Hosson, J.T.M. Influence of random roughness on the Casimir force at small separations. *Phys. Rev. B* **2008**, *77*, 075412.

[33] Broer, W.; Palasantzas, G.; Knoester, J.; Svetovoy, V.B. Roughness correction to the Casimir force at short separations: Contact distance and extreme value statistics. *Phys. Rev. B* **2012**, *85*, 155410.

[34] Bulgac, A.; Magierski, P.; Wirzba, A. Scalar Casimir effect between Dirichlet spheres or a plate and a sphere. *Phys. Rev. D* **2006**, *73*, 025007.

[35] Emig, T.; Jaffe, R.L.; Kardar, M.; Scardicchio, A. Casimir Interaction between a Plate and a Cylinder. *Phys. Rev. Lett.* **2006**, *96*, 080403.

[36] Bordag, M. Casimir effect for a sphere and a cylinder in front of a plane and corrections to the proximity force theorem. *Phys. Rev. D* **2006**, *73*, 125018.

[37] Emig, T.; Graham, N.; Jaffe, R.L.; Kardar, M. Casimir Forces Between Arbitrary Compact Objects. *Phys. Rev. Lett.* **2007**, *99*, 170403.

[38] Kenneth, O.; Klich, I. Casimir forces in a T-operator approach. *Phys. Rev. B* **2008**, *78*, 014103.

[39] Emig, T.; Graham, N.; Jaffe, R.L.; Kardar, M. Casimir forces between compact objects: The scalar case. *Phys. Rev. D* **2008**, *77*, 025005.

[40] Rahi, S.J.; Emig, T.; Graham, N.; Jaffe, R.L.; Kardar, M. Scattering theory approach to electromagnetic Casimir forces. *Phys. Rev. D* **2009**, *80*, 085021.

[41] Maia Neto, P.A.; Lambrecht, A.; Reynaud, S. Casimir energy between a plane and a sphere in electromagnetic vacuum. *Phys. Rev. A* **2008**, *78*, 012115.

[42] Canaguier-Durand, A.; Maia Neto, P.A.; Caverio-Pelaez, I.; Lambrecht, A.; Reynaud, S. Casimir Interaction between Plane and Spherical Metallic Surfaces. *Phys. Rev. Lett.* **2009**, *102*, 230404.

[43] Fosco, C.D.; Lombardo, F.C.; Mazzitelli, F.D. Proximity force approximation for the Casimir energy as a derivative expansion. *Phys. Rev. D* **2011**, *84*, 105031.

[44] Bimonte, G.; Emig, T.; Jaffe, R.L.; Kardar, M. Casimir forces beyond the proximity force approximation. *EPL* **2012**, *97*, 50001.

[45] Bimonte, G.; Emig, T.; Kardar, M. Material dependence of Casimir force: Gradient expansion beyond proximity. *Appl. Phys. Lett.* **2012**, *100*, 074110.

[46] Teo, L.P. Material dependence of Casimir interaction between a sphere and a plate: First analytic correction beyond proximity force approximation. *Phys. Rev. D* **2013**, *88*, 045019.

[47] Bimonte, G. Going beyond PFA: A precise formula for the sphere-plate Casimir force. *EPL* **2017**, *118*, 20002.

[48] Hartmann, M.; Ingold, G.-L.; Maia Neto, P.A. Plasma versus Drude Modeling of the Casimir Force: Beyond the Proximity Force Approximation. *Phys. Rev. Lett.* **2017**, *119*, 043901.

[49] Spreng, B.; Hartmann, M.; Henning, V.; Maia Neto, P.A.; Ingold, G.-L. Proximity force approximation and specular reflection: Application of the WKB limit of Mie scattering to the Casimir effect. *Phys. Rev. A* **2018**, *97*, 062504.

[50] Hartmann, M.; Ingold, G.-L.; Maia Neto, P.A. Advancing numerics for the Casimir effect to experimentally relevant aspect ratios. *Phys. Scr.* **2018**, *93*, 114003.

[51] Speake, C.C.; Trenkel, C. Forces between Conducting Surfaces due to Spatial Variations of Surface Potential. *Phys. Rev. Lett.* **2003**, *90*, 160403.

[52] Behunin, R.O.; Intravaia, F.; Dalvit, D.A.R.; Maia Neto, P.A.; Reynaud, S. Modeling electrostatic patch effects in Casimir force measurements. *Phys. Rev. A* **2012**, *85*, 012504.

[53] Behunin, R.O.; Dalvit, D.A.R.; Decca, R.S.; Genet, C.; Jung, I.W.; Lambrecht, A.; Liscio, A.; López, D.; Reynaud, S.; Schnoering, G.; et al. Kelvin probe force microscopy of metallic surfaces used in Casimir force measurements. *Phys. Rev. A* **2014**, *90*, 062115.

[54] Pirozhenko, I.; Lambrecht, A.; Svetovoy, V.B. Sample dependence of the Casimir force. *New J. Phys.* **2006**, *8*, 238.

[55] Svetovoy, V.B.; van Zwol, P.J.; Palasantzas, G.; De Hosson, J.T.M. Optical properties of gold films and the Casimir force. *Phys. Rev. B* **2008**, *77*, 035439.

[56] Decca, R.S.; López, D.; Osquigui, E. New results for the Casimir interaction: Sample characterization and low temperature measurements. *Int. J. Mod. Phys. A* **2010**, *25*, 2223–2230.

[57] Bimonte, G. Making precise predictions of the Casimir force between metallic plates via a weighted Kramers-Kronig transform. *Phys. Rev. A* **2011**, *83*, 042109.

[58] Esquivel, R.; Svetovoy, V.B. Correction to the Casimir force due to the anomalous skin effect. *Phys. Rev. A* **2004**, *69*, 062102.

[59] Svetovoy, V.B.; Esquivel, R. Nonlocal impedances and the Casimir entropy at low temperatures. *Phys. Rev. E* **2005**, *72*, 036113.

[60] Sernelius, B.E. Effects of spatial dispersion on electromagnetic surface modes and on modes associated with a gap between two half spaces. *Phys. Rev. B* **2005**, *71*, 235114.

[61] Mostepanenko, V.M. Casimir Puzzle and Conundrum: Discovery and Search for Resolution. *Universe* **2021**, *7*, 84.

[62] Torgerson, J.R.; Lamoreaux, S.K. Low-frequency character of the Casimir force between metallic films. *Phys. Rev. E* **2004**, *70*, 047102.

[63] Bimonte, G. Comment on “Low-frequency character of the Casimir force between metallic films”. *Phys. Rev. E* **2006**, *73*, 048101.

[64] Intravaia, F.; Henkel, C. Casimir Interaction from Magnetically Coupled Eddy Currents *Phys. Rev. Lett.* **2009**, *103*, 130405.

[65] Intravaia, F.; Ellingsen, S.A.; Henkel, C. Casimir-Foucault interaction: Free energy and entropy at low temperature. *Phys. Rev. A* **2010**, *82*, 032504.

[66] Svetovoy, V.B.; Esquivel, R. The Casimir free energy in high- and low-temperature limits. *J. Phys. A Math. Gen.* **2006**, *39*, 6777–6784.

[67] Klimchitskaya, G.L.; Mostepanenko, V.M.; Svetovoy, V.B. Probing the response of metals to low-frequency s-polarized evanescent waves. *Europhys. Lett.* **2022**, *139*, 66001.

[68] Klimchitskaya, G.L.; Mostepanenko, V.M.; Svetovoy, V.B. *Experimentum crusis* for electromagnetic response of metals to evanescent waves and the Casimir puzzle. *Universe* **2022**, *8*, 574.

[69] Klimchitskaya, G.L.; Mostepanenko, V.M. Casimir effect invalidates the Drude model for transverse electric evanescent waves. *Physics* **2023**, *5*, 952–967.

[70] Törmä, P.; Barnes, W.L. Strong coupling between surface plasmon polaritons and emitters: A review. *Rep. Progr. Phys.* **2015**, *78*, 013901.

[71] Hsu, J.W.P. Near-field scanning optical microscopy studies of electronic and photonic materials and devices. *Mater. Sci. Engin R Rep.* **2001**, *33*, 1–50.

[72] Aigouy, L.; Lahrech, A.; Grésillon, S.; Cory, H.; Bocvara, A.C.; Rivoal, J.C. Polarization effects in apertureless scanning near-field optical microscopy: An experimental study. *Opt. Lett.* **1999**, *24*, 187–189.

[73] Culshaw, W.; Jones, D.S. Effect of a Metal Plate on Total Reflection. *Proc. Phys. Soc. B* **1953**, *66*, 859–864.

[74] Brady, J.J.; Brick, R.O.; Pearson, V.D. Penetration of Microwaves into the Rarer Medium in Total Reflection. *J. Opt. Soc. Am.* **1960**, *50*, 1080–1084.

[75] Zhu, S.; Yu, A.W.; Hawley, D.; Roy, R. Frustrated total internal reflection: A demonstration and review. *Am. J. Phys.* **1986**, *54*, 601–606.

[76] Dhital, M.; Klimchitskaya, G.L.; Mostepanenko, V.M.; Mohideen, U. Measurement of the unusual dielectric response to low-frequency s-polarized evanescent waves in metals with implications for the Casimir effect. *EPL* **2025**, *151*, 26002.

[77] Banishev, A.A.; Chang, C.-C.; Klimchitskaya, G.L.; Mostepanenko, V.M.; Mohideen, U. Measurement of the gradient of the Casimir force between a nonmagnetic gold sphere and a magnetic nickel plate. *Phys. Rev. B* **2012**, *85*, 195422.

[78] Banishev, A.A.; Klimchitskaya, G.L.; Mostepanenko, V.M.; Mohideen, U. Demonstration of the Casimir Force between Ferromagnetic Surfaces of a Ni-Coated Sphere and a Ni-Coated Plate. *Phys. Rev. Lett.* **2013**, *110*, 137401.

[79] Banishev, A.A.; Klimchitskaya, G.L.; Mostepanenko, V.M.; Mohideen, U. Casimir interaction between two magnetic metals in comparison with nonmagnetic test bodies. *Phys. Rev. B* **2013**, *88*, 155410.

[80] Bimonte, G.; López, D.; Decca, R.S. Isoelectronic determination of the thermal Casimir force. *Phys. Rev. B* **2016**, *93*, 184434.

[81] Lambrecht, A.; Reynaud, S. Casimir force between metallic mirrors. *Eur. Phys. J. D* **2000**, *8*, 309–318.

[82] Ordal, M.A.; Bell, R.J.; Alexander Jr., R.W.; Long, L.L.; Querry, M.R. Optical properties of fourteen metals in the infrared and far infrared: Al, Co, Cu, Au, Fe, Pb, Mo, Ni, Pd, Pt, Ag, Ti, V, and W. *Appl. Opt.* **1985**, *24*, 4493–4499.

[83] Vonsovskii, S.V. *Magnetism*; Wiley: New York, 1974.

[84] Timsit, R.S. High Speed Electronic Connector Design: A Review of Electrical and Electromagnetic Properties of Passive Contact Elements – Part 1. *IEICE Trans. Electron.* **2008**, *E91-C*, 1178–1191.

[85] Glathart, J.L. The inner, initial, magnetic permeability of iron and nickel at ultra-high radiofrequencies. *Phys. Rev.* **1939**, *55*, 833–838.

[86] Hoag, J.B.; Glathart, J.L. The outer, initial permeability of nickel from 10 to 70 megacycles. *Phys. Rev.* **1940**, *57*, 240.

[87] Nonaka, Y.; Nakane, H.; Maeda, T.; Hasuike, K. Simultaneous measurement of the resistivity and permeability of a film sample with a double coil. *IEEE Trans. Instrum. Meas.* **1995**, *44*, 679–682.

[88] Geyer, B.; Klimchitskaya, G.L.; Mostepanenko, V.M. Thermal Casimir interaction between two magnetodielectric plates. *Phys. Rev. B* **2010**, *81*, 104101.

[89] Lucyszyn, S. Microwave characterization of nickel. *PIERS Online* **2008**, *4*, 686–690.

[90] Ellingsen, S.A., Frequency spectrum of the Casimir force: interpretation and a paradox. *Europhys. Lett.* **2008**, *82*, 53001.

[91] Hasegawa, H. Frequency-Dependent Electrical Conductivity of Nearly and Weakly Ferromagnetic Metals Deviations from Drude's Formula. *J. Phys. Soc. Japan* **1979**, *46*, 831–838.

[92] Maebashi, H.; Miyake, K. Effects of orbital correlation on Drude weight in ferromagnetic metallic phase of $\text{La}_{1-x}\text{Sr}_x\text{MnO}_3$. *Physica B: Cond. Matt.* **2000**, *281*282, 526–527.

[93] Eric Yang, S.-R.; Sinova, J.; Jungwirth, T.; Shim, Y.P.; MacDonald, A.H. Non-Drude optical conductivity of (III, Mn)V ferromagnetic semiconductors. *Phys. Rev. B* **2003**, *67*, 045205.

[94] Chudnovsky, E.M. Theory of Spin Hall Effect: Extension of the Drude Model. *Phys. Rev. Lett.* **2007**, *99*, 206601.

[95] Wolff, C.; Rodrguez-Oliveros, R.; Busch, K. Simple magnetooptic transition metal models for timedomain simulations. *Opt. Express* **2013**, *21*, 12022–12037.

[96] Hoang, D.-T.; Diep, H.T. Spin Transport in Magnetically Ordered Systems: Ferromagnets, Antiferromagnets and Frustrated Systems. *Condens. Matter* **2023**, *8*, 3.

[97] Shee, P.; Halder, T.; Yang, C.-J.; Tickoo, N.; Samal, R.; Kulkarni, R.; Pandey, S.K.; Kashid, V.; Nandy, A.K.; Thamizhavel, A.; Mukherjee, A.; Pal, S. The interplay of magnetic order with the electronic scattering and crystal-field effects in a metallic ferromagnet. ArXiv:2512.12996 [cond-mat.str-el].

[98] Klimchitskaya, G.L.; Mostepanenko, V.M. Quantum field theoretical framework for the electromagnetic response of graphene and dispersion relations with implications to the Casimir effect. *Phys. Rev. D* **2023**, *107*, 105007.

[99] Klimchitskaya, G.L.; Mostepanenko, V.M. Temperature Dependence of the Response Functions of Graphene: Impact on Casimir and CasimirPolder Forces in and out of Thermal Equilibrium. *Physics* **2025**, *7*, 44.

[100] Klimchitskaya, G.L.; Mostepanenko, V.M. An alternative response to the off-shell quantum fluctuations: A step forward in resolution of the Casimir puzzle. *Eur. Phys. J. C* **2020**, *80*, 900.

[101] Klimchitskaya, G.L.; Mostepanenko, V.M. Casimir effect for magnetic media: Spatially non-local response to the off-shell quantum fluctuations. *Phys. Rev. D* **2021**, *104*, 085001.

[102] Klimchitskaya, G.L.; Mostepanenko, V.M. Theory-experiment comparison for the Casimir force between metallic test bodies: A spatially non-local dielectric response. *Phys. Rev. A* **2022**, *105*, 012805.

[103] Hannemann, M.; Wegner, G.; Henkel, C. No-Slip Boundary Conditions for Electron Hydrodynamics and the Thermal Casimir Pressure. *Universe* **2021**, *7*, 108.

[104] Henkel, C. Electromagnetic response of the electron gas and the thermal Casimir pressure anomaly. *Int. J. Mod. Phys. A* **2025**, *40*, 2543007.